ACS APPLIED MATERIALS & INTERFACES

Research Article

www.acsami.org

Solution Processed Titanyl Phthalocyanines as Donors in Solar Cells: Photoresponse to 1000 nm

Mayank Mayukh, Mariola R. Macech, Diogenes Placencia, Yu Cao, Neal R. Armstrong, and Dominic V. McGrath*

Department of Chemistry and Biochemistry, University of Arizona, Tucson, Arizona 85721-0041, United States

Supporting Information

ABSTRACT: We report a route to thin-film polymorphs of soluble TiOPc derivatives that exhibit similar near-IR absorptivities as vapor deposited thin-films of the parent TiOPc chromophore (phase-I and phase-II polymorphs) and demonstrate that solution-processed planar and bulk heterojunction solar cells fabricated with one of these derivatives exhibited photoactivity throughout the same near-IR wavelength range without compromising V_{OC}. Solution-processed thin-films of soluble octakis(alkylthio)-substituted TiOPc derivatives **1**−**3** exhibit absorption extending to 1000 nm. When incorporated into OPV devices, the contributions from the lowest CT excitonic state (Q_B band) of **1** to device performance were evident in both PHJ and BHJ architectures, indicating sufficient driving force for PIET. This contribution was improved via intimate mixing of donor and acceptor molecules in a BHJ architecture, albeit with a decrease in efficiency. IPCE of the best performing BHJ device revealed a contribution from **1** exceeding that of acceptor PCBM, and extending to 1000 nm.

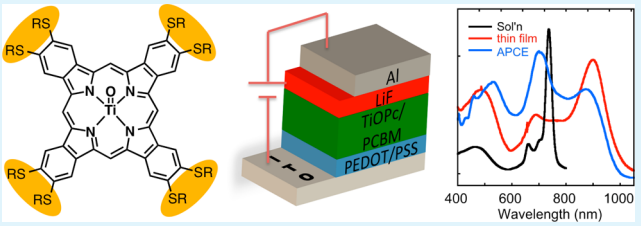

KEYWORDS: *organic photovoltaic, near-infrared, organic thin films, polymorphs, X-ray diffraction*

INTRODUCTION

The efficiency of organic photovoltaics (OPVs) is limited by the light absorption of the active layer, which is confined to the visible region for most chromophores, while 50% of the AM1.5G solar irradiance is incident in the near-IR region (700−1400 nm). Among the challenges remaining to achieve high OPVs efficiencies, at the module level, are (1) extending the spectral response of the OPV to the near-IR, taking advantage of the full AM1.5 solar irradiance and (2) achieving this near-IR response while keeping the open-circuit photopotential (V_{OC}) high. Significant progress has been made in improving the efficiency of both planar and bulk heterojunction (PHJ, BHJ) OPVs, and 7−12% power conversion efficiency (PCE) research cells are now possible with both polymer and small molecule active layers, but these devices still do not have appreciable absorbance beyond ∼800 nm.[1−13] If thin-film absorptivities can be extended to the near-IR with no significant loss of V_{OC}, a significant improvement in PCE can be anticipated.

Titanyl phthalocyanine (TiOPc, Figure 1a)[14,15] could provide an excellent platform for small molecule active materials with extended near-IR response and has recently been explored in OPVs.[16−20] TiOPc is one of several tri- and tetravalent Pcs such as ClAlPc[21−24] and ClInPc,[23−25] the nonplanarity and dipolar character of which[26,27] lead to several known crystalline polymorphs (e.g., amorphous TiOPc, Phase I, Phase II, and the Y Phase), some of which exhibit Q-band absorbance well into the near-IR region[19,28] and significantly improved photoelectrical activity (Figure 1).[29−33] The

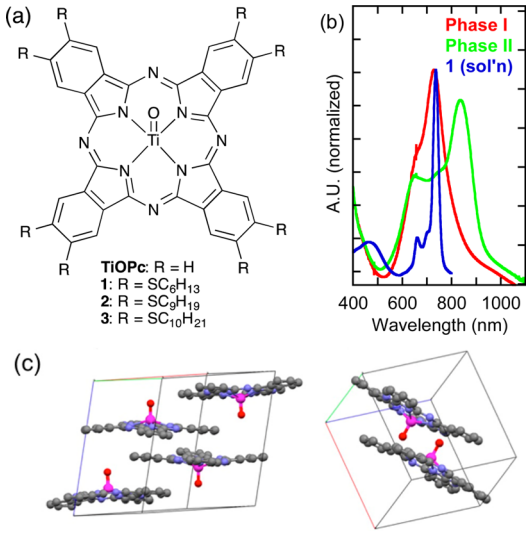

Figure 1. (a) Structures of TiOPc and modified TiOPcs **1**−**3**. (b) Absorption spectra of phase-I and phase-II polymorphs TiOPc and for comparison a solution spectrum of **1**. (c) Molecular arrangement in phase-I (left) and phase-II (right) of crystalline TiOPc.

Received: July 3, 2015
Accepted: October 9, 2015

ACS Publications © XXXX American Chemical Society

DOI: 10.1021/acsami.5b05900
ACS Appl. Mater. Interfaces XXXX, XXX, XXX−XXX

extensively red-shifted thin-film Q-band spectra as well as high ionization potential (IP), which, associated with C_{60} as an electron acceptor, has led to OPVs with V_{OC} from 0.8−1.0 V.[25,34]

TiOPc, however, is particularly insoluble,[15] necessitating relatively expensive and inherently low-throughput vapor deposition techniques to produce near-IR absorbing thin-films, precluding its incorporation into solution-processed devices.[16−20] Solution-processing methods can deposit thin-films over large areas using techniques such as reel-to-reel wet coating, inkjet printing, and spin-coating.[35,36] While specific TiOPc polymorphs, phase-II in particular, have been obtained by varying vapor deposition processing conditions,[26,33,37−44] *all prior efforts at polymorph control in solution-processed thin films of soluble versions of TiOPc have not produced the desired near-IR absorbing phases.*[32,33] This lack of control in obtaining the desired polymorphs limits the use of soluble TiOPc derivatives as active materials in solution processed OPVs and in related molecular electronic device platforms.

We herein report the first solvent processing route to near-IR-absorbing thin-film polymorphs of soluble versions of TiOPc, providing materials that absorb out to 1000 nm. The optical properties of these films are reminiscent of phase-I and -II polymorphs of crystalline TiOPc, the latter of which strongly absorbs in the near-IR (Figure 1b). We further demonstrate that the ensemble properties[45] of these materials can be exploited in PHJ OPVs that are active for solar-electric conversion across this same near-IR wavelength range.

RESULTS AND DISCUSSION

The absorption spectrum for parent TiOPc thin-films is characterized by the presence of two Q-bands at ∼690 nm (Q_A) and ∼830 nm (Q_B) depending on the crystalline phases present (Figure 1b). Though the origin of the longer wavelength Q_B band has been a matter of debate,[28,46,47] it is generally accepted that a close $\pi-\pi$ contact of adjacent Pcs leads to charge-transfer (CT) character of the exitonic states of the near-IR absorption.[48] Because of the relatively short intermolecular distances between adjacent TiOPc molecules observed in both convex and concave pairs of their triclinic unit cell (Figure 1c), TiOPc Phase-II has a higher probability for exciton dissociation and higher charge (hole) mobility necessary for increased OPV efficiency.[49] Theoretical models[49] and photoconductivity studies with TiOPc[31,48,50−52] predict that enhanced exciton diffusion lengths and charge mobilities occur in staggered cofacial geometries of Pc/Nc aggregates in general.[53]

We envisioned that substitution of TiOPc at the peripheral positions with alkylthio groups would introduce solubility, shift the absorption profile to the near-IR, and possibly provide secondary sulfur−sulfur noncovalent interactions that could influence the molecular arrangement of the chromophores in the condensed phase.[54,55] Since close $\pi-\pi$ contact of the TiOPc chromophores in the condensed phase is necessary for attaining the near-IR absorbing Q_B-band, a balance between steric crowding and solubility provided by the alkylthio groups could be achieved by varying the alkyl chain lengths.

In this context we investigated the thin-film and powder morphologies of a series octakis(alkylthio)-substituted TiOPc derivatives (**1**−**3**) that were prepared using a solvent-free method we recently reported.[56] Alkylthio substitution of TiOPc at the peripheral positions is known to increase solubility and bathochromically shift the absorption profile;[56−59] in dilute solution, the Q-band of **1**−**3** appears at 736 nm,[56] about 36 nm red-shifted relative to the unmodified TiOPc chromophore (Figure 1b).[28]

The condensed phase absorption spectra of TiOPc derivatives **1**−**3** drop-cast from $CHCl_3$ solutions onto quartz substrates provided a clear indication of the presence of phase-II type polymorphs (Figure S2a). A Q_A-band at ∼690 nm, slightly blue-shifted with respect to the solution spectrum, was accompanied by a Q_B-band at ∼890 nm, significantly red-shifted with respect to the solution spectrum, that can be attributed to the formation of close $\pi-\pi$ contacts in the Pc aggregates similar to the phase-II polymorph of crystalline TiOPc.[28,60] A similar, albeit less pronounced Q_B-band was observed in thin-films of **1**−**3** spin-coated from $CHCl_3$ onto poly(3,4-ethylenedioxythio-phene):polystyrenesulfonate coated ITO (PEDOT:PSS/ITO), a more device relevant substrate (Figure 2a).

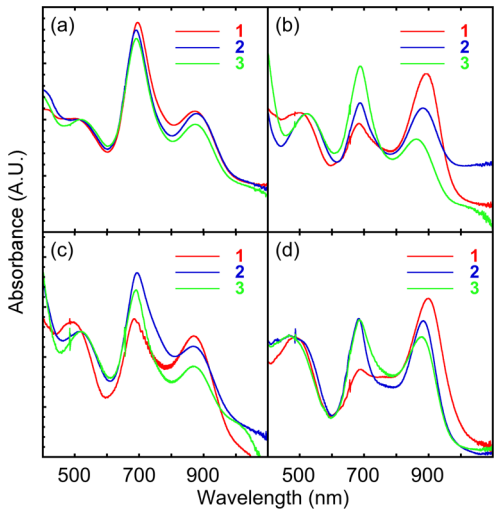

Figure 2. Absorption spectra of alkylthio TiOPcs **1**−**3** in thin-films. Thin-films spin-coated from (a) $CHCl_3$ on PEDOT:PSS/ITO (pristine); (b) ODCB on PEDOT:PSS/ITO substrate (pristine); (c) ODCB on PEDOT:PSS/ITO substrate (annealed at 150 °C for 50 min); and (d) MDCB on quartz (pristine).

We observed a more dramatic enhancement of the Q_B band when aromatic solvents, such as *o*-dichlorobenzene (ODCB), were used for spin-coating **1**−**3** on PEDOT:PSS/ITO substrates (Figure 2b). Unlike the films cast from $CHCl_3$ solution on either quartz or PEDOT:PSS/ITO, the relative ratios of the Q_A and the Q_B bands were strongly influenced by the substituent chain lengths of **1**−**3**. TiOPc derivatives **1** and **2** showed a more intense Q_B band relative to the Q_A band, while **3** showed an absorption spectrum similar to that of the films spin-coated from $CHCl_3$ on PEDOT:PSS/ITO. Thermal annealing of the films at 150 °C led to a decreased Q_B band absorptivity for **1**−**3** (Figure 2c). Films with an absorbance profile most clearly reminiscent of the phase-II polymorph of crystalline TiOPc were obtained by spin-coating from *m*-dichlorobenzene (MDCB)(Figure 2d).

The presence of Q_A and Q_B bands for **1**−**3** and the variable enhancements of the Q_B band under certain film-forming conditions suggested a similar origin of these two bands to those observed in phase-I and -II polymorphs of the parent TiOPc chromophore.[14,28] To verify the presence and identity of the two polymorphs we investigated the crystal packing in

DOI: 10.1021/acsami.5b05900
ACS Appl. Mater. Interfaces XXXX, XXX, XXX−XXX

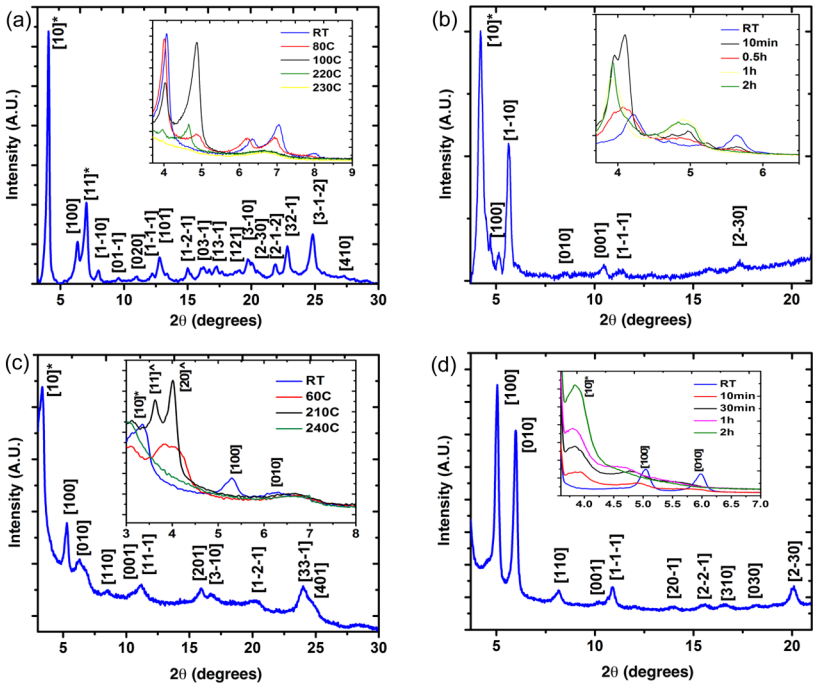

Figure 3. X-ray diffractogram for TiOPc derivatives: (a) RT powder of **1** with (inset) variable temperature (VT) powder of 1; (b) RT thin-film (cast from ODCB on PEDOT:PSS/ITO) of **1** with (inset) annealing (150 °C) thin-film of **1**; (c) RT powder of **2** with (inset) VT powder of **2**; and (d) RT thin-film (cast from ODCB on PEDOT:PSS/ITO) of **2** with (inset) annealing (150 °C).

TiOPc derivatives **1** and **2** by X-ray diffraction (XRD). The powder X-ray diffractograms for both **1** and **2** indicate the presence of a mixture of Col_{hex}[61−64] and triclinic unit cells (Figure 3a, 3c). The [10] and [11] peaks in the powder diffractograms at 4.3° and 7.3° in **1**, and the [10] peak at 3.38° in **2** indicate a Col_{hex} phase. The remaining peaks in the powder diffractograms in both **1** and **2** can be fit into triclinic unit cells.

During thermal annealing, the high angle peaks in the powder diffractograms of **1** and **2** gradually disappeared and only the low angle peaks, suggestive of a Col[62−65] phase, were observed at ∼100 and 60 °C, respectively. For example, upon annealing a powder sample of **1**, we observed transformation to a Col_{rec} phase between 80 and 100 °C (Figure 3a inset). The presence of a Col_{rec} phase was supported by [20] and [11] peaks at ∼4° and 4.9° between 100 and 210 °C. Similarly, the powder diffractogram for **2** exhibited an unresolved broad peak at ∼3.8° between 60 and 200 °C (Figure 3c inset). At 210 °C, the 3.8° peak transformed into [20] and [11] peaks at 3.6° and 4.1° indicating transformation to a Col_{rec} phase. The broad peak at ∼6.8° seen in diffractograms at high temperatures indicated loss of order in powder samples.

The diffractogram at room temperature for thin-films of **1** revealed the presence of a mixture of Col_{hex} and triclinic unit cells, consistent with the studies on the powder samples (Figure 3b). The [10] peak at ca. 4.2° in **1** was indicative of the presence of Col_{hex} unit cells. The presence of Col_{hex} phase supported the presence of *H*-type aggregates that resulted in a slightly blue-shifted Q_A-band relative to the solution phase *Q*-band absorption in **1**.[66] On the basis of the remaining peaks, we proposed triclinic unit cells for **1** (Table 1). The room temperature diffractogram for thin-films of **2** revealed the presence of a single, triclinic unit cell (Figure 3d). However, a short coherence length can explain the absence of the Col_{hex} phase in the room temperature diffractogram for thin-films of **2** since a [10] peak at 3.8°, corresponding to the Col_{hex} phase, appeared after just 10 min of thermal annealing (Figure 3d, inset).

Table 1. Lattice Parameters from the XRD[a] of 1 and 2

Cmpd	Col_{hex} parameters	Triclinic parameters
1[b]	a = 23.8 Å	a = 14.0 Å, b = 16.4 Å, c = 9.8 Å α = 104.5°, β = 104.9°, γ = 91.5° V = 2100 Å^3
1[c]	a = 23.7 Å	a = 23.0 Å, b = 16.1 Å, c = 8.6 Å α = 85.3°, β = 94.4°, γ = 132.2° V = 2378.7 Å^3
2[b]	a = 30.3 Å	a = 16.8 Å, b = 15.3 Å, c = 8.9 Å α = 113.8°, β = 94.2°, γ = 91.5° V = 2074.3 Å^3
2[c]		a = 17.9 Å, b = 15.6 Å, c = 9.0 Å α = 71.1°, β = 95.7°, γ = 96.1° V = 2340.8 Å^3

[a]Data for RT diffractograms. For data on annealed samples, see Supporting Information. [b]Powder. [c]Thin-film from ODCB on PEDOT:PSS/ITO.

Indeed, short intermolecular $\pi-\pi$ distances, comparable to that of the parent TiOPc and responsible for the near-IR absorbing Q_B-band,[28] were realized along the *c* axis in the powder diffractograms for both **1** and **2**. Upon annealing the thin-films of **1** and **2**, the peaks corresponding to the triclinic unit cell disappeared, consistent with the studies on the powder samples as well as the thin-film absorption studies (vide infra). For example, [20] and [10] peaks at 3.9° and 4.8° indicative of a Col_{rec} phase, and a [10] peak at 3.8° indicative of a Col_{hex} phase were observed in the thin-film diffractograms for **1** (Figure 3b inset) and **2** (Figure 3d inset), respectively. The loss of a triclinic unit cell upon annealing explains the relative decrease in the Q_B-band intensity of the annealed thin-films of **1** and **2** (Figure S2f). The presence of a Col_{rec} phase in **1** is

DOI: 10.1021/acsami.5b05900
ACS Appl. Mater. Interfaces XXXX, XXX, XXX−XXX

indicative of a stronger core to core interaction in **1** relative to **2**, as a result of shorter side chains.[64]

We evaluated **1** as a potential donor in OPVs. PHJ devices were fabricated from both pristine and annealed films of **1** spin-coated from ODCB onto PEDOT:PSS/ITO, the absorption spectra of which appeared as in Figure 2b for the pristine **1** film, with an enhanced Q_B band, and as in Figure 2c for the annealed **1** film. We modulated the donor-layer thickness by varying the concentration of the solution of **1**, measuring film thicknesses by AFM (Table 2). Subsequent vapor deposition of C_{60}, bathocuprine (BCP), and aluminum completed the devices with pristine (devices 1 and 3) and thermally annealed (devices 2 and 4) films of **1**, the device parameters of which are summarized in Table 2.

Table 2. Device Parameters for OPVs Based on 1

device[a]	conc. (mg/mL)	l^b (nm)	V_{OC} (V)	J_{SC} (mA/cm^2)	FF	η^c (%)
planar heterojunction devices[d]						
1	3.5	21	0.39	3.17	0.40	0.78
2	3.5	23[e]	0.49	2.10	0.34	0.53
3	5.5	28	0.35	3.29	0.55	0.97
4	5.5	34[e]	0.40	2.15	0.50	0.66
bulk heterojunction devices[d]						
5	6[f]	31	0.17	0.33	0.31	0.02
6	12[f]	40	0.55	0.50	0.40	0.11
7	18[f]	72	0.38	0.29	0.35	0.04
8	12[g]	91	0.65	1.07	0.45	0.31
9	18[g]	121	0.71	0.46	0.26	0.08
10	18[g]	149	0.41	0.47	0.36	0.07

[a]Device area = 0.019 cm^2. Thickness of PEDOT:PSS layer = 108 nm. [b]Thickness of the donor layer for PHJ and the active layer for BHJ OPV devices. [c]PCE was derived from the equation: $\eta = (J_{sc}V_{oc}FF)/P_0$; J_{sc} = short-circuit current, V_{oc} = open-circuit voltage, FF = fill-factor, and P_0 = incident-light intensity =65.5 mW/cm^2. [d]PHJ OPV device: ITO/PEDOT:PSS/**1**/C60/BCP/Al. BHJ OPV device: ITO/PEDOT:PSS/**1**:PCBM/LiF/Al. [e]Film (ITO/PEDOT:PSS/**1**) annealed at 150 °C for 10 min. [f]**1**/PCBM ratio = 1:1 (w/w). [g]**1**/PCBM ratio = 1:3 (w/w).

The PHJ devices of **1**/C_{60} had relatively low efficiencies, yet exhibited device parameters consistent with processing conditions and, more importantly, solar-electric conversion activity within the absorption range of **1** (vide infra). Device 1, with a donor-layer thickness of ~21 nm, exhibited a V_{OC} and a J_{SC} of 0.39 V and 3.17 mA/cm^2, respectively, with a η of 0.78%. Upon increasing the donor-layer thickness to 28 nm (device 3), the V_{OC} decreased to 0.35 V, while a slight increase in the J_{SC} to 3.29 mA/cm^2 was observed. The higher efficiency for device 3 compared to device 1 can be attributed to the increased fill factor (FF) from 0.40 to 0.55. Devices 2 and 4 from respective annealed films of **1** showed correspondingly lower J_{SC} and FF but a higher V_{OC} (Figure 4a). This observation is consistent with planarization of the donor film during thermal annealing, leading to less current because of a decrease in the interfacial surface area between the donor and the acceptor, and an increase in photopotential due to a reduction in pinholes, as evident from the lowering of the leakage current at reverse bias, which is linked to increases in the shunt resistance, R_p[67,68] (Figure 4b). Further, the lower performance of the devices from the annealed films, which exhibit decreased Q_B (increased Q_A) bands relative to pristine films (cf., Figures 2b and c), is consistent with higher photoactivity for the Q_B band. Higher photoactivity for phase-II compared to phase-I TiOPc has been observed for vacuum-deposited PHJ OPV devices from unmodified TiOPc.[19,20]

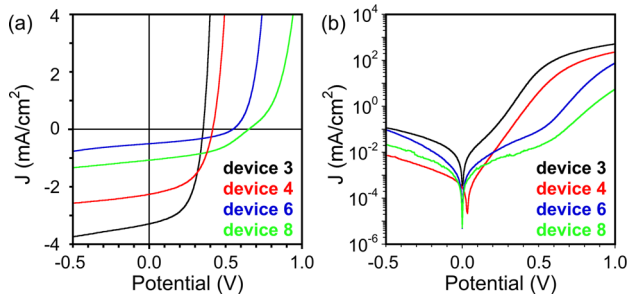

Figure 4. (a) $J-V$ (light current) and (b) semilog (dark current) plots for **1**/C60 PHJ OPV devices (3 and 4) and **1**/PCBM BHJ devices (6 and 8). Devices 4 and 8 are annealed and show lower reverse saturation current than corresponding pristine devices 3 and 6.

We fabricated BHJ OPV devices by spin-coating, under ambient atmosphere, a solution of **1** and phenyl-C61-butyric acid methyl ester (PCBM) in $CHCl_3$ onto PEDOT:PSS-coated, detergent–solvent-cleaned ITO, followed by vacuum deposition of LiF and aluminum, in sequence, to complete the device. The **1**/PCBM blended films showed absorption with a band at ~400 nm, typical of PCBM, as well as the Q_A and Q_B bands of **1** at ~690 and 875 nm, respectively, similar to those observed in the pristine films of **1** (Figure S5), suggesting that the PCBM did not cause significant disruption of intermolecular interactions in **1**. Active layers of different thicknesses were prepared by spin coating a solution of **1** and PCBM of varying concentrations (Table 2) and imaged using AFM. The morphology of the thin-films were dependent on the **1**/PCBM ratio. For a **1**/PCBM ratio of 1:1 (w/w), AFM images revealed large, spherical domains of ca. 450 nm diameter with rms surface roughness of 8 nm (Figure 5a). However, thin-films from a **1**/PCBM ratio of 1:3 (w/w) were relatively smooth, with absence of large domains (Figure 5b). This pattern of phase-segregation remained invariant irrespective of the film thickness (Figure S6).

We observed an enhancement of V_{OC} upon intimate mixing of donor and acceptor in these BHJ devices, as well as a greater relative contribution of the CT band of **1** to device efficiency (vide infra). Device 5, with an active layer thickness of ~31 nm for **1**/PCBM ratio of 1:1 (w/w), exhibited a low V_{OC} value of 0.17 mV suggesting the presence of pin-holes in the relatively thin-film. Upon increasing the thickness to 40 nm in device 6, we observed an increase in J_{SC}, V_{OC}, and FF (Table 2, device 5 → 6). Further increase in thickness to 72 nm in device 7 led to decreased J_{SC}, V_{OC}, and FF, indicating the active layer thickness exceeded the exciton diffusion length. Deviation from **1**/PCBM ratio of 1:1 (w/w) to 3:1 did not lead to a working device. However, when we used a **1**/PCBM ratio of 1:3 (w/w) in a 91 nm thick active-layer (device 8), a significant increase in both V_{OC} and J_{SC} to 0.65 V and 1.07 mA, respectively, was observed. Increasing the active layer thickness to 121 nm in device 9 led to increased V_{OC}, however both J_{SC} and *FF* decreased significantly reflecting limited charge mobility. The V_{OC} for devices 8 and 9 are comparable to the V_{OC} of the PHJ devices fabricated from vacuum-deposited TiOPc.[19,20]

Annealing of the active layer led to a significant lowering of the V_{OC} in device 10. Certainly, the balance between optical absorption and charge recombination was met for devices with

DOI: 10.1021/acsami.5b05900
ACS Appl. Mater. Interfaces XXXX, XXX, XXX–XXX

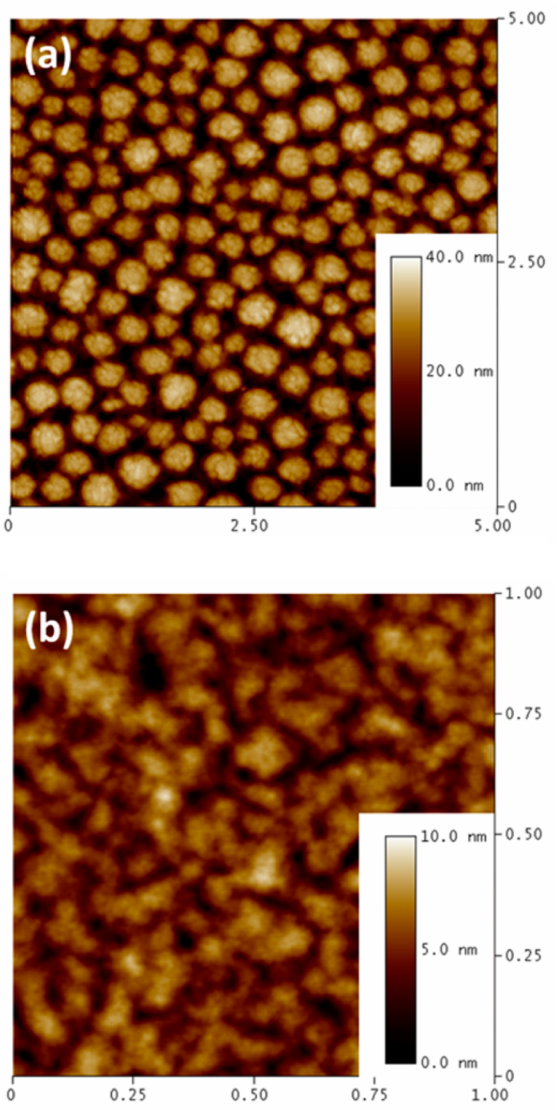

Figure 5. AFM height images for active layer thin-film with **1**:PCBM ratio of (a) 1:1 and (b) 1:3.

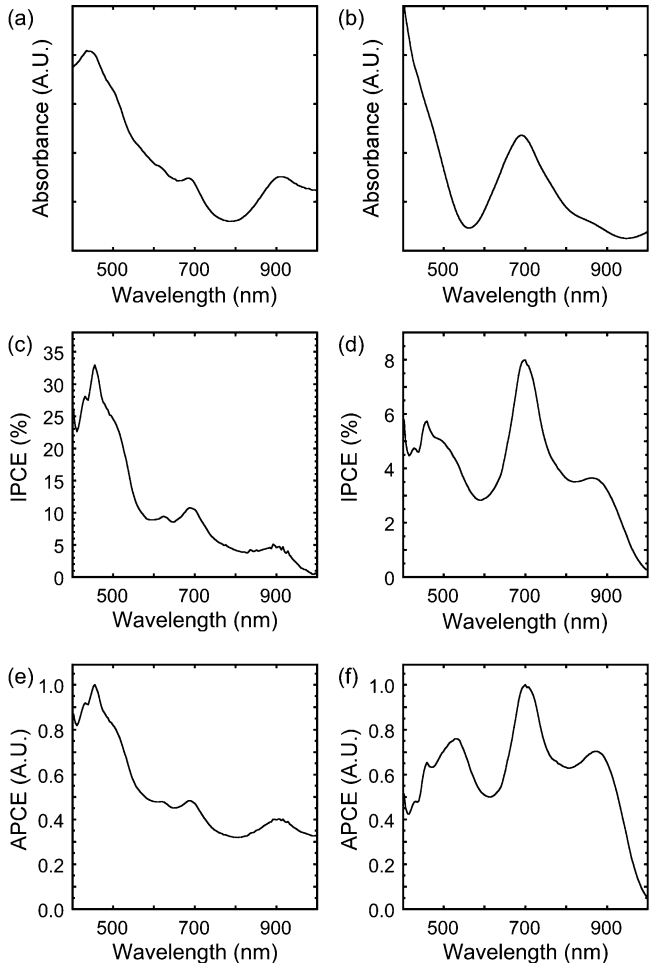

Figure 6. Absorbance (a, b) and incident-photon (c, d) and absorbed-photon (e, f) current efficiency (IPCE, APCE) measurements for PHJ device 3 (left) and BHJ device 8 (right).

active layer thicknesses of 40 and 91 nm, for **1**/PCBM ratios of 1:1 and 1:3, respectively. The *J*−*V* and semilog plot for the best performing devices 6 and 8 are shown in Figure 4. The lower performance of the devices from **1**/PCBM ratio of 1:1 (w/w) can be attributed to the formation of unfavorable large domains of **1** observed in the AFM, which can serve as sites for recombination (Figure 5).[69]

Quantum efficiency measurements on the best performing PHJ OPV (device 3) verifies the photon-to-electron conversion extending to 1 μm (Figure 6). The absorbance spectrum for device 3 exhibited a panchromatic absorption which is an overlay of the C_{60} absorption band (400−600 nm) and the Q_A and Q_B band absorptions of **1** (600−1000 nm) (Figure 6a). Incident photon to current efficiency (IPCE) measurements were done on a device of area 0.125 cm^2 inside a stainless steel sealed vessel under a nitrogen atmosphere. Absorbed photon to current efficiency (APCE) was calculated using the IPCE data and the absorbance (transmittance) spectrum for the OPVs along the transparent region near the OPVs. The APCE/IPCE spectra revealed contributions from **1** in the near-IR region with local maxima around 680 and 920 nm, corresponding to the Q_A and Q_B bands of **1**. The maximum absorbed and incident photon-to-electron conversion around 450 nm corresponds to C_{60}, consistent with its higher absorbance in the device. The relatively lower contributions from the Q_A and Q_B bands toward IPCE/APCE spectra suggests recombination of excitons.[70]

Analogous quantum efficiency measurements for the best performing BHJ OPV device 8 revealed a much higher relative proportion of photon-to-electron conversion for **1** than PCBM. The shapes of the IPCE/APCE and the device absorption spectra were significantly different (Figure 6). While the absorbance spectrum of the device showed higher contribution from PCBM than **1** (Figure 6b), the relative contributions to the IPCE from **1** exceed that of PCBM (Figure 6d). Moreover, there is an enhancement of the Q_B band in relation to the Q_A band when comparing the IPCE to the absorption of the device. This is further manifested in the APCE in which the Q_B band results in a large fraction of the internal quantum efficiency of the device (Figure 6f). Hence, despite the relatively low predominance of the Q_B-absorbing polymorph in the active layer, relatively efficient APCE in this region indicates sufficient driving force for photoinduced electron transfer (PIET) for this lowest energy CT excitonic state.

DOI: 10.1021/acsami.5b05900
ACS Appl. Mater. Interfaces XXXX, XXX, XXX−XXX

CONCLUSION

We have demonstrated that incorporation of solution-processed donor films of a soluble TiOPc derivative into OPVs can extend the photoactivity to 1 μm in the near-IR without compromising V_{OC}. We have developed a route to thin-film polymorphs of soluble TiOPc derivatives that exhibit similar near-IR absorptivities as vapor deposited thin-films of the parent TiOPc chromophore (phase-I and phase-II polymorphs). The contributions from the lowest CT excitonic state of **1** (Q_B band) to device performance were evident in both PHJ and BHJ architecture devices, indicating sufficient driving force for PIET. This contribution is improved via intimate mixing of donor and acceptor molecules in a BHJ architecture, albeit with a decrease in efficiency. IPCE of the best performing BHJ device 8 revealed a contribution from **1** exceeding that of PCBM, and extending to 1000 nm. These studies complement our previous work on polymorph control in vacuum deposited TiOPc donor layers by solvent annealing, and these results may be enhanced by developing related materials with improved charge mobilities. The approach presented here may prove a general method for extending the solar-electric conversion window with materials that have enhanced near-IR absorption in the condensed phase.

ASSOCIATED CONTENT

Supporting Information

The Supporting Information is available free of charge on the ACS Publications website at DOI: 10.1021/acsami.5b05900.

Experimental details and spectroscopic, microscopy, and X-ray diffraction data for **1**–**3** (PDF)

AUTHOR INFORMATION

Corresponding Author

*E-mail: mcgrath@u.arizona.edu.

Notes

The authors declare no competing financial interest.

ACKNOWLEDGMENTS

This research was supported as part of the Center for Interface Science: Solar-Electric Materials (CIS:SEM), an Energy Frontier Research Center funded by the U.S. Department of Energy, Office of Science, Office of Basic Energy Sciences under Award Number DE-SC0001084 (N.R.A., M.R.M., Y.C., D.P. and materials), and the National Science Foundation Award Number CHE-0719437 (D.V.M., M.M.).

REFERENCES

(1) Gilles, D.; Scharber, M. C.; Brabec, C. J. Polymer-Fullerene Bulk-Heterojunction Solar Cells. *Adv. Mater.* **2009**, *21*, 1323–1338.

(2) Liang, Y. Y.; Yu, L. P. A New Class of Semiconducting Polymers for Bulk Heterojunction Solar Cells with Exceptionally High Performance. *Acc. Chem. Res.* **2010**, *43*, 1227–1236.

(3) Liang, Y.; Xu, Z.; Xia, J.; Tsai, S. T.; Wu, Y.; Li, G.; Ray, C.; Yu, L. For the Bright Future—Bulk Heterojunction Polymer Solar Cells with Power Conversion Efficiency of 7.4%. *Adv. Mater.* **2010**, *22*, E135–E138.

(4) Guo, X. G.; Zhou, N. J.; Lou, S. J.; Smith, J.; Tice, D. B.; Hennek, J. W.; Ortiz, R. P.; Navarrete, J. T. L.; Li, S. Y.; Strzalka, J.; Chen, L. X.; Chang, R. P. H.; Facchetti, A.; Marks, T. J. Polymer Solar Cells with Enhanced Fill Factors. *Nat. Photonics* **2013**, *7*, 825–833.

(5) Hammond, M. R.; Kline, R. J.; Herzing, A. A.; Richter, L. J.; Germack, D. S.; Ro, H. W.; Soles, C. L.; Fischer, D. A.; Xu, T.; Yu, L. P.; Toney, M. F.; DeLongchamp, D. M. Molecular Order in High-Efficiency Polymer/Fullerene Bulk Heterojunction Solar Cells. *ACS Nano* **2011**, *5*, 8248–8257.

(6) Huang, J. H.; Hsiao, Y. S.; Richard, E.; Chen, C. C.; Chen, P. L.; Li, G.; Chu, C. W.; Yang, Y. The Investigation of Donor-Acceptor Compatibility in Bulk-Heterojunction Polymer Systems. *Appl. Phys. Lett.* **2013**, *103*, 043304.

(7) Lou, S. J.; Szarko, J. M.; Xu, T.; Yu, L. P.; Marks, T. J.; Chen, L. X. Effects of Additives on the Morphology of Solution Phase Aggregates Formed by Active Layer Components of High-Efficiency Organic Solar Cells. *J. Am. Chem. Soc.* **2011**, *133*, 20661–20663.

(8) Small, C. E.; Chen, S.; Subbiah, J.; Amb, C. M.; Tsang, S. W.; Lai, T. H.; Reynolds, J. R.; So, F. High-Efficiency Inverted Dithienogermole-Thienopyrrolodione-Based Polymer Solar Cells. *Nat. Photonics* **2012**, *6*, 115–120.

(9) Son, H. J.; Carsten, B.; Jung, I. H.; Yu, L. P. Overcoming Efficiency Challenges in Organic Solar Cells: Rational Development of Conjugated Polymers. *Energy Environ. Sci.* **2012**, *5*, 8158–8170.

(10) You, J. B.; Dou, L. T.; Yoshimura, K.; Kato, T.; Ohya, K.; Moriarty, T.; Emery, K.; Chen, C. C.; Gao, J.; Li, G.; Yang, Y. A Polymer Tandem Solar Cell with 10.6% Power Conversion Efficiency. *Nat. Commun.* **2013**, *4*, 1446.

(11) Kyaw, A. K. K.; Wang, D. H.; Gupta, V.; Leong, W. L.; Ke, L.; Bazan, G. C.; Heeger, A. J. Intensity Dependence of Current-Voltage Characteristics and Recombination in High-Efficiency Solution-Processed Small-Molecule Solar Cells. *ACS Nano* **2013**, *7*, 4569–4577.

(12) Kyaw, A. K. K.; Wang, D. H.; Gupta, V.; Zhang, J.; Chand, S.; Bazan, G. C.; Heeger, A. J. Efficient Solution-Processed Small-Molecule Solar Cells with Inverted Structure. *Adv. Mater.* **2013**, *25*, 2397–2402.

(13) Kyaw, A. K. K.; Wang, D. H.; Wynands, D.; Zhang, J.; Nguyen, T. Q.; Bazan, G. C.; Heeger, A. J. Improved Light Harvesting and Improved Efficiency by Insertion of an Optical Spacer (ZnO) in Solution-Processed Small-Molecule Solar Cells. *Nano Lett.* **2013**, *13*, 3796–3801.

(14) Hiller, W.; Strahle, J.; Kobel, W.; Hanack, M. Synthesis and Properties of New One-Dimensional Conductors. 14. Polymorphism, Conductivity and Crystal-Structure of Oxo-Phthalocyaninato Titanium(IV). *Z. Kristallogr.* **1982**, *159*, 173–183.

(15) Taube, R. Über Titanphthalocyanine. *Z. Chem.* **1963**, *3*, 194–194.

(16) Tsuzuki, T.; Shirota, Y.; Rostalski, J.; Meissner, D. The Effect of Fullerene Doping on Photoelectric Conversion Using Titanyl Phthalocyanine and a Perylene Pigment. *Sol. Energy Mater. Sol. Cells* **2000**, *61*, 1–8.

(17) Tsuzuki, T.; Hirota, N.; Noma, N.; Shirota, Y. Photoelectrical Conversion of p-n Heterojunction Devices Using Thin Films of Titanyl Phthalocyanine and a Perylene Pigment. *Thin Solid Films* **1996**, *273*, 177–180.

(18) Brumbach, M.; Placencia, D.; Armstrong, N. R. Titanyl Phthalocyanine/C60 Heterojunctions: Band-Edge Offsets and Photovoltaic Device Performance. *J. Phys. Chem. C* **2008**, *112*, 3142–3151.

(19) Placencia, D.; Wang, W.; Shallcross, R. C.; Nebesny, K. W.; Brumbach, M.; Armstrong, N. R. Organic Photovoltaic Cells Based on Solvent-Annealed, Textured Titanyl Phthalocyanine/C60 Heterojunctions. *Adv. Funct. Mater.* **2009**, *19*, 1913–1921.

(20) Placencia, D.; Wang, W.; Gantz, J.; Jenkins, J. L.; Armstrong, N. R. Highly Photoactive Titanyl Phthalocyanine Polymorphs as Textured Donor Layers in Organic Solar Cells. *J. Phys. Chem. C* **2011**, *115*, 18873–18884.

(21) Bailey-Salzman, R. F.; Rand, B. P.; Forrest, S. R. Near-Infrared Sensitive Small Molecule Organic Photovoltaic Cells Based on Chloroaluminum Phthalocyanine. *Appl. Phys. Lett.* **2007**, *91*, 013508.

(22) Ioannidis, A.; Dodelet, J. P. Hole and Electron Transport in Chloroaluminum Phthalocyanine Thin Films. *J. Phys. Chem. B* **1997**, *101*, 5100–5107.

(23) Ioannidis, A.; Dodelet, J. P. Hole Mobilities in Trivalent Metal Phthalocyanine Thin Films. 2. Anomalous Mobility Temperature Dependence in The Low-Temperature Region 213–93 K for

DOI: 10.1021/acsami.5b05900
ACS Appl. Mater. Interfaces XXXX, XXX, XXX–XXX

Chloroaluminum, Chlorogallium, and Chloroindium Phthalocyanine Thin Films. *J. Phys. Chem. B* **1997**, *101*, 901−907.
(24) Xu, M. S.; Xu, J. B.; Tian, D. X.; Ji, Z. G.; Chen, H. Z.; Wang, M.; Que, D. L. Alternate Heteroepitaxial Growth of Chloroindium Phthalocyanine and Chloroaluminum Phthalocyanine Ultrathin Multilayered Structure and Its Xerographic and Optical Properties. *Thin Solid Films* **2001**, *384*, 109−114.
(25) Wang, W.; Placencia, D.; Armstrong, N. R. Planar and Textured Heterojunction Organic Photovoltaics Based On Chloroindium Phthalocyanine (ClInPc) Versus Titanyl Phthalocyanine (Tiopc) Donor Layers. *Org. Electron.* **2011**, *12*, 383−393.
(26) Kera, S.; Okudaira, K. K.; Harada, Y.; Ueno, N. Molecular Orientation and Aggregation of Titanyl Phthalocyanine Molecules on Graphite Substrates: Effects of Surface Topography of the Substrate. *Japan. J. Appl. Phys. 1* **2001**, *40*, 783−787.
(27) Fukagawa, H.; Hosoumi, S.; Yamane, H.; Kera, S.; Ueno, N. Dielectric Properties of Polar-Phthalocyanine Monolayer Systems with Repulsive Dipole Interaction. *Phys. Rev. B: Condens. Matter Mater. Phys.* **2011**, *83*, 085304.
(28) Mizuguchi, J.; Rihs, G.; Karfunkel, H. R. Solid-State Spectra of Titanylphthalocyanine as Viewed from Molecular Distortion. *J. Phys. Chem.* **1995**, *99*, 16217−16227.
(29) Klofta, T.; Linkous, C.; Armstrong, N. R. Photoelectrochemical Studies of Vanadyl Phthalocyanine (Vopc) Thin-Film Electrodes. *J. Electroanal. Chem. Interfacial Electrochem.* **1985**, *185*, 73−92.
(30) Klofta, T. J.; Danziger, J.; Lee, P.; Pankow, J.; Nebesny, K. W.; Armstrong, N. R. Photoelectrochemical and Spectroscopic Characterization of Thin Films of Titanyl Phthalocyanine: Comparisons with Vanadyl Phthalocyanine. *J. Phys. Chem.* **1987**, *91*, 5646−5651.
(31) Liang, D. J.; Peng, W. L.; Wang, Y. Solvent-Stabilized Y-Type Oxotitanium Phthalocyanine Photoconductive Nanoparticles: Preparation and Application in Single-Layered Photoreceptors. *Adv. Mater.* **2012**, *24*, 5249−5253.
(32) Haisch, P.; Winter, G.; Hanack, M.; Luer, L.; Egelhaaf, H. J.; Oelkrug, D. Soluble Alkyl- and Alkoxy-Substituted Titaniumoxo Phthalocyanines: Synthesis and Photoconductivity. *Adv. Mater.* **1997**, *9*, 316.
(33) Winter, G.; Heckmann, H.; Haisch, P.; Eberhardt, W.; Hanack, M.; Luer, L.; Egelhaaf, H. J.; Oelkrug, D. Study of Substituent Effects On The Photoconductivity of Soluble 2,(3)- and 1,(4)-Substituted Phthalocyaninato- and Naphthalocyaninatotitanium(IV) Oxides. *J. Am. Chem. Soc.* **1998**, *120*, 11663−11673.
(34) Williams, G.; Sutty, S.; Klenkler, R.; Aziz, H. Renewed Interest in Metal Phthalocyanine Donors for Small Molecule Organic Solar Cells. *Sol. Energy Mater. Sol. Cells* **2014**, *124*, 217−226.
(35) Krebs, F. C. Roll-to-Roll Fabrication of Monolithic Large-Area Polymer Solar Cells Free from Indium-Tin-Oxide. *Sol. Energy Mater. Sol. Cells* **2009**, *93*, 1636−1641.
(36) Krebs, F. C. All Solution Roll-to-Roll Processed Polymer Solar Cells Free from Indium-Tin-Oxide and Vacuum Coating Steps. *Org. Electron.* **2009**, *10*, 761−768.
(37) Conboy, J. C.; Olson, E. J. C.; Adams, D. M.; Kerimo, J.; Zaban, A.; Gregg, B. A.; Barbara, P. F. Impact of Solvent Vapor Annealing on the Morphology and Photophysics of Molecular Semiconductor Thin Films. *J. Phys. Chem. B* **1998**, *102*, 4516−4525.
(38) Yao, J. C.; Yonehara, H.; Pac, C. J. A Convenient Synthetic Method for Pure Oxo(Phthalocyaninato)Titanium(Iv) and Application to Other Metal Phthalocyanines. *Bull. Chem. Soc. Jpn.* **1995**, *68*, 1001−1005.
(39) Ghosez, P.; Cote, R.; Gastonguay, L.; Veilleux, G.; Denes, G.; Dodelet, J. P. Characterization of a Highly Photoactive Molecular Semiconductor - Oxotitanium Phthalocyanine. *Chem. Mater.* **1993**, *5*, 1581−1590.
(40) Liu, C. Y.; Bard, A. J. In-Situ Regrowth and Purification by Zone Melting of Organic Single-Crystal Thin Films Yielding Significantly Enhanced Optoelectronic Properties. *Chem. Mater.* **2000**, *12*, 2353−2362.
(41) Yamashita, A.; Maruno, T.; Hayashi, T. Phase-Selective Formation of Titanylphthalocyanine Thin Films by Organic Molecular Beam Deposition. *J. Phys. Chem.* **1994**, *98*, 12695−12701.
(42) Walzer, K.; Toccoli, T.; Pallaoro, A.; Iannotta, S.; Wagner, C.; Fritz, T.; Leo, K. Comparison of Organic Thin Films Deposited by Supersonic Molecular-Beam Epitaxy and Organic Molecular-Beam Epitaxy: The Case of Titanyl Phthalocyanine. *Surf. Sci.* **2006**, *600*, 2064−2069.
(43) Coppede, N.; Toccoli, T.; Pallaoro, A.; Siviero, F.; Walzer, K.; Castriota, M.; Cazzanelli, E.; Iannotta, S. Polymorphism and Phase Control in Titanyl Phthalocyanine Thin Films Grown by Supersonic Molecular Beam Deposition. *J. Phys. Chem. A* **2007**, *111*, 12550−12558.
(44) Del Cano, T.; Parra, V.; Rodriguez-Mendez, M. L.; Aroca, R. F.; De Saja, J. A. Characterization of Evaporated Trivalent and Tetravalent Phthalocyanines Thin Films: Different Degree of Organization. *Appl. Surf. Sci.* **2005**, *246*, 327−333.
(45) Henson, Z. B.; Mullen, K.; Bazan, G. C. Design Strategies for Organic Semiconductors Beyond the Molecular Formula. *Nat. Chem.* **2012**, *4*, 699−704.
(46) Saito, T.; Sisk, W.; Kobayashi, T.; Suzuki, S.; Iwayanagi, T. Photocarrier Generation Processes of Phthalocyanines Studied by Photocurrent and Electroabsorption Measurements. *J. Phys. Chem.* **1993**, *97*, 8026−8031.
(47) Popovic, Z. D.; Khan, M. I.; Atherton, S. J.; Hor, A. M.; Goodman, J. L. Study of Carrier Generation in Titanyl Phthalocyanine (TiOPc) by Electric-Field-Induced Quenching of Integrated and Time-Resolved Fluorescence. *J. Phys. Chem. B* **1998**, *102*, 657−663.
(48) Nakai, K.; Ishii, K.; Kobayashi, N.; et al. Theoretical Calculations of the Electronic Absorption Spectra of Oxotitanium(IV) Phthalocyanine in the Solid State. *J. Phys. Chem. B* **2003**, *107*, 9749−9755.
(49) Norton, J. E.; Bredas, J. L. Theoretical characterization of titanyl phthalocyanine as a p-type organic semiconductor: Short Intermolecular π-π Interactions Yield Large Electronic Couplings and Hole Transport Bandwidths. *J. Chem. Phys.* **2008**, *128*, 034701.
(50) Brinkmann, M.; Wittmann, J. C.; Barthel, M.; Hanack, M.; Chaumont, C. Highly Ordered Titanyl Phthalocyanine Films Grown by Directional Crystallization on Oriented Poly(Tetrafluoroethylene) Substrate. *Chem. Mater.* **2002**, *14*, 904−914.
(51) Gulbinas, V. Transient Absorption of Photoexcited Titanylphthalocyanine in Various Molecular Arrangements. *Chem. Phys.* **2000**, *261*, 469−479.
(52) Zhou, J.; Mi, J.; Zhu, R. Y.; Li, B.; Qian, S. X. Ultrafast Excitation Relaxation in Titanylphthalocyanine Thin Film. *Opt. Mater.* **2004**, *27*, 377−382.
(53) Tant, J.; Geerts, Y. H.; Lehmann, M.; De Cupere, V.; Zucchi, G.; Laursen, B. W.; Bjornholm, T.; Lemaur, V.; Marcq, V.; Burquel, A.; Hennebicq, E.; Gardebien, F.; Viville, P.; Beljonne, D.; Lazzaroni, R.; Cornil, J. Liquid Crystalline Metal-Free Phthalocyanines Designed for Charge and Exciton Transport. *J. Phys. Chem. B* **2005**, *109*, 20315−20323.
(54) Crivillers, N.; Mas-Torrent, M.; Bromley, S. T.; Wurst, K.; Veciana, J.; Rovira, C. Influence of Intermolecular Interactions on the Formation of Tetra(carbomethoxy)-tetrathiafulvalene Assemblies. *ChemPhysChem* **2007**, *8*, 1565−1571.
(55) Di Maria, F.; Olivelli, P.; Gazzano, M.; Zanelli, A.; Biasiucci, M.; Gigli, G.; Gentili, D.; D'Angelo, P.; Cavallini, M.; Barbarella, G. A Successful Chemical Strategy To Induce Oligothiophene Self-Assembly into Fibers with Tunable Shape and Function. *J. Am. Chem. Soc.* **2011**, *133*, 8654−8661.
(56) Mayukh, M.; Sema, C. M.; Roberts, J. M.; McGrath, D. V. Solvent-Free Synthesis of Soluble, Near-IR Absorbing Titanyl Phthalocyanine Derivatives. *J. Org. Chem.* **2010**, *75*, 7893−7896.
(57) Arslanoglu, Y.; Hamuryudan, E. Synthesis and Derivatization of Near-IR Absorbing Titanylphthalocyanines with Dimethylaminoethylsulfanyl Substituents. *Dyes Pigm.* **2007**, *75*, 150−155.
(58) Kimura, T.; Kumasaka, J.; Namauo, T. Preparation, Structure Determination, and Electrochemical Properties of Bis-{[1,4,8,11,15,18,22,25-octaethyl-2,3,9,10,16,17,23,24-octakis-

DOI: 10.1021/acsami.5b05900
ACS Appl. Mater. Interfaces XXXX, XXX, XXX−XXX

(methylthio)phthalocyaninato]titanium(IV)} Benzene-1,2,4,5-tetrathiolate. *Eur. J. Org. Chem.* **2008**, *2008*, 5079−5084.
(59) Kobayashi, N.; Ogata, H.; Nonaka, N.; Luk'yanets, E. A. Effect of Peripheral Substitution on the Electronic Absorption and Fluorescence Spectra of Metal-Free and Zinc Phthalocyanines. *Chem. - Eur. J.* **2003**, *9*, 5123−5134.
(60) Hernandez, J.; Choi, S. I. Optical Absorption by Charge-Transfer Excitons in Linear Molecular Crystals. *J. Chem. Phys.* **1969**, *50*, 1524−1532.
(61) Sergeyev, S.; Pisula, W.; Geerts, Y. H. Discotic Liquid Crystals: A New Generation of Organic Semiconductors. *Chem. Soc. Rev.* **2007**, *36*, 1902−1929.
(62) Chandrasekhar, S. Liquid Crystals of Disklike Molecules. *Adv. Liq. Cryst.* **1982**, *5*, 47−78.
(63) Schweicher, G.; Gbabode, G.; Quist, F.; Debever, O.; Dumont, N.; Sergeyev, S.; Geerts, Y. H. Homeotropic and Planar Alignment of Discotic Liquid Crystals: The Role of the Columnar Mesophase. *Chem. Mater.* **2009**, *21*, 5867−5874.
(64) Laschat, S.; Baro, A.; Steinke, N.; Giesselmann, F.; Hagele, C.; Scalia, G.; Judele, R.; Kapatsina, E.; Sauer, S.; Schreivogel, A.; Tosoni, M. Discotic Liquid Crystals: From Tailor-Made Synthesis to Plastic Electronics. *Angew. Chem., Int. Ed.* **2007**, *46*, 4832−4887.
(65) Binnemans, K.; Lodewyckx, K.; Cardinaels, T.; Parac - Vogt, T. N.; Bourgogne, C.; Guillon, D.; Donnio, B. Dinuclear Lanthanide Schiff-Base Complexes Forming a Rectangular Column Mesophase. *Eur. J. Inorg. Chem.* **2006**, *2006*, 150−157.
(66) Kasha, M. R.; Rawls, H. R.; Ashraf El-Bayoumi, M. The Exciton Model in Molecular Spectroscopy. *Pure Appl. Chem.* **1965**, *11*, 371−392.
(67) Zhou, Y.; Khan, T. M.; Shim, J. W.; Dindar, A.; Fuentes-Hernandez, C.; Kippelen, B. All-Plastic Solar Cells with a High Photovoltaic Dynamic Range. *J. Mater. Chem. A* **2014**, *2*, 3492−3497.
(68) Yoo, S.; Domercq, B.; Kippelen, B. Intensity-Dependent Equivalent Circuit Parameters of Organic Solar Cells Based on Pentacene and C60. *J. Appl. Phys.* **2005**, *97*, 103706.
(69) Tamayo, A. B.; Dang, X. D.; Walker, B.; Seo, J.; Kent, T.; Nguyen, T. Q. A Low Band Gap, Solution Processable Oligothiophene with a Dialkylated Diketopyrrolopyrrole Chromophore for Use in Bulk Heterojunction Solar Cells. *Appl. Phys. Lett.* **2009**, *94*, 103301.
(70) Mayerhoffer, U.; Deing, K.; Gruss, K.; Braunschweig, H.; Meerholz, K.; Wurthner, F. Outstanding Short-Circuit Currents in BHJ Solar Cells Based on NIR-Absorbing Acceptor-Substituted Squaraines. *Angew. Chem., Int. Ed.* **2009**, *48*, 8776−8779.

DOI: 10.1021/acsami.5b05900
ACS Appl. Mater. Interfaces XXXX, XXX, XXX−XXX